Available online at www.sciencedirect.com
SCIENCE DIRECT
Journal of Catalysis 233 (2005) 464–477
JOURNAL OF CATALYSIS
www.elsevier.com/locate/jcat

Ethanol steam reforming over $Mg_xNi_{1-x}Al_2O_3$ spinel oxide-supported Rh catalysts

Fabien Aupretre [a], Claude Descorme [a,1], Daniel Duprez [a,*], Dominique Casanave [b], Denis Uzio [b]

[a] *Laboratoire de Catalyse en Chimie Organique (LACCO), 40, Av. Recteur Pineau, 86022 Poitiers cedex, France*
[b] *Institut Français du Pétrole (IFP), Vernaison, France*

Received 10 March 2005; revised 6 May 2005; accepted 9 May 2005

Available online 21 June 2005

Abstract

Two series of Rh/spinel catalysts supported on alumina were prepared. In the first series, magnesium, nickel, and aluminum nitrates were co-impregnated over γ-alumina beads (200 $m^2\,g^{-1}$), dried, and further calcined at 1000 °C to obtain $Mg_xNi_{1-x}Al_2O_4/Al_2O_3$ supports ($\approx$100 $m^2\,g^{-1}$), where x ranged from 0 to 1. These supports were impregnated with aqueous solutions of Rh nitrate to obtain 0.1–0.2 wt% Rh catalysts. We prepared the second series by coating alumina beads with Mg acetate. The support was dried and calcined at 1000 °C. The $MgAl_2O_4$ spinel was formed by solid–solid reaction between magnesia and alumina. $MgAl_2O_4$ was impregnated with different Rh precursor salts (nitrate, chloride, acetate) to obtain 0.2–0.8 wt% Rh loading. Supports and catalysts were characterized by BET area, pore volume, XRD, TEM and SEM, CO_2 chemisorption (basicity), and dimethyl-3,3-but-1-ene isomerization (acidity). Rh dispersion was measured by H_2 chemisorption. The second series of catalysts was also characterized by FTIR of adsorbed lutidine and DRIFT. The activity of the catalysts was evaluated in the ethanol steam reforming at 700 °C under 1 or 11 atm (H_2O/ethanol molar ratio of 4, space velocity 24,000 h^{-1}). Acidic and basic properties of the catalysts are crucial parameters inasmuch as they control the primary selectivity for ethylene or acetaldehyde. To avoid ethylene formation, which leads to a significant carbon deposit, all acidic sites should be neutralized. The effects of the precursors used in the support and catalyst preparation were investigated. The second preparation method gave less acidic materials with very high performances (activity and stability) in the ethanol steam reforming reaction. The morphology of the support, with a Mg-deficient spinel layer (thickness of about 8–9 nm) intimately covering all of the alumina grains (around 40 nm in size), can explain the neutralization of most acidic sites. Nitrate precursors should be avoided, since as we obtained the most acidic materials and the poorest stability. Rh acetate led to neutral catalysts with interesting performances in the ethanol steam reforming, and Rh chloride allowed the preparation of well-dispersed Rh catalysts. Although the catalysts prepared with Rh chloride were moderately acidic, they were very active and stable.

Keywords: Hydrogen production; Ethanol; Biofuels; Rhodium; $MgAl_2O_4$; Spinel oxides; Basicity

1. Introduction

Over the last several years, hydrogen production from renewable fuels has attracted interest because of the potential applications in proton exchanged membrane fuel cells (PEMFC). Such a technology combines both a significant net reduction in the yield of CO_2 as a by-product, because of the utilization of biofuels and the excellent energy conversion yield in fuel cells. Hydrogen can be produced by steam reforming (fuel + H_2O) or autothermal reforming (O_2 is added to equilibrate the endothermicity of the steam reforming reaction). Steam reforming of bioethanol has been widely investigated because (i) it can be produced from renewable resources in large production units; (ii) in contrast to methanol, ethanol toxicity is low; and (iii) bioethanol is virtually sulfur-free, which is crucial for processes involving metal-based catalysts. Nickel catalysts [1–10] were investi-

* Corresponding author. Fax: +33-5-49-45-34-99.
E-mail address: daniel.duprez@univ-poitiers.fr (D. Duprez).
[1] Present address: Institut de Recherches sur la Catalyse, 2, Av. Albert Einstein, 69626 Villeurbanne cedex, France.

0021-9517/$ – see front matter
doi:10.1016/j.jcat.2005.05.007

gated in detail because of the relatively good activity of Ni in the steam reforming processes. Ni was shown to rapidly deactivate because of coke formation, but copper is known as a strong inhibitor of coke formation, and thus nickel–copper bimetallic catalysts were specially designed and studied to avoid such a deactivation [11–16]. Cobalt catalysts have also exhibited good performance in hydrogen production from ethanol reforming [17–24]. However, the rapid sintering of these catalysts generally limited the application to the reactions performed at moderate temperatures. Noble metals, especially Rh and Pt [1,5,25–39], were also investigated. It was shown that Rh was the most active metal in the ethanol steam reforming, as for the steam reforming of many hydrocarbons [40–45].

Ethanol steam reforming consists of three main reactions accounting for the formation of H_2, CO_2, CO, and CH_4:

$$C_2H_5OH + 3H_2O \rightarrow 2CO_2 + 6H_2, \quad \Delta H^0_{298} = +174\ \mathrm{kJ\,mol^{-1}}, \tag{1}$$

$$C_2H_5OH + H_2O \rightarrow 2CO + 4H_2, \quad \Delta H^0_{298} = +256\ \mathrm{kJ\,mol^{-1}}, \tag{2}$$

$$C_2H_5OH + 2H_2 \rightarrow 2CH_4 + H_2O, \quad \Delta H^0_{298} = -157\ \mathrm{kJ\,mol^{-1}}. \tag{3}$$

Carbon monoxide is favored at high temperatures, and methane is thermodynamically favored at low temperatures. Three main parameters may affect the H_2 yield at equilibrium (Y_{H_2}): temperature (T), total pressure (P), initial H_2O/ethanol molar ratio (R). Y_{H_2} increases with T and R and decreases with P. At $P = 1$ bar and for $R = 3$, Y_{H_2} reaches a maximum around 700 °C. However, increasing the total pressure may be necessary to adapt the reformer to the global process conditions, especially when hydrogen purification involves a Pd–Ag membrane. In such a case, a working pressure of 8–15 bar is required.

Four other reactions can also occur: ethanol dehydrogenation to acetaldehyde (4), ethanol dehydration to ethylene (5), and ethanol cracking to carbon dioxide and methane (6) or carbon monoxide, methane, and hydrogen (7):

$$C_2H_5OH \rightarrow CH_3CHO + H_2, \quad \Delta H^0_{298} = +68\ \mathrm{kJ\,mol^{-1}}, \tag{4}$$

$$C_2H_5OH \rightarrow C_2H_4 + H_2O, \quad \Delta H^0_{298} = +45\ \mathrm{kJ\,mol^{-1}}, \tag{5}$$

$$C_2H_5OH \rightarrow \tfrac{1}{2}CO_2 + \tfrac{3}{2}CH_4, \quad \Delta H^0_{298} = -74\ \mathrm{kJ\,mol^{-1}}, \tag{6}$$

$$C_2H_5OH \rightarrow CO + CH_4 + H_2, \quad \Delta H^0_{298} = +49\ \mathrm{kJ\,mol^{-1}}. \tag{7}$$

Reaction (6) is strongly favored at low temperatures. In fact, calculations showed that CO_2 and CH_4 are the only products thermodynamically favored at low temperature ($T < 200$ °C), with a stoichiometry equal to that of reaction (6) ($CH_4/CO_2 = 3$) [5]. However, many studies have shown that acetaldehyde and ethylene may form at relatively low temperatures, well before the formation of hydrogen and CO_x by reactions (1) and (2). Compared with the steam reforming reaction, the ethanol dehydrogenation and dehydration reactions are much faster, and acetaldehyde and ethylene may be considered important intermediates in the formation of hydrogen [5,37]. The support plays a crucial role in the steam reforming reaction: (i) it may favor water splitting into OH groups and promote the migration of these reactive species toward the metal particles, where the final steps of the CO_x and hydrogen formation occur [43,46–49]; (ii) it may catalyze reaction (4) and/or (5) and affect the selectivity for the final products [5,12,20,35,50,51]; and (iii) it may finally contribute to the stabilization of the metal particles at high temperature under steam [22,52–57]. Alumina-based supports are often used in the steam reforming reaction because they offer a good compromise between the different roles the support should play. However, at high temperature under steam, a slow migration of the Rh ionic species can occur and lead to an irreversible deactivation. This is due to the fact that transition aluminas present an open spinel structure with a high number of vacancies that can host and stabilize ionic species of the metals [58–63]. The catalyst is then virtually irreducible and loses its activity, especially in steam reforming reactions. The aim of this study is to describe the preparation and characterization of Rh catalysts deposited on alumina-supported $Mg_xNi_{1-x}Al_2O_3$ spinel oxides for application in ethanol steam reforming at 700 °C under moderate pressure (11 bar). With vacancies of alumina filled with Mg^{2+} or Ni^{2+} ions, it is expected that Rh can be stabilized in the fully reduced form. Insofar as dehydration and dehydrogenation have a great impact on the selectivity (H_2, CO_x, CH_4) and on the catalyst stability (ethylene is a major precursor of coke), much attention was paid to the acidic and basic properties of the catalysts.

2. Experimental

2.1. Preparation

Two series of supports and catalysts were prepared. In every case, the starting material consisted of γ-alumina beads (200 $m^2\,g^{-1}$, main impurities Na, Fe, Si < 500 ppm, 1–2 mm in diameter) provided by Rhodia.

In the first series, the spinel supports were prepared by coimpregnation of magnesium, nickel, and aluminum nitrates (Alpha Aesar) in the molar ratio $x/(1-x)/2$ for Mg/Ni/Al. The amount of salts was adjusted to obtain 5 wt% Mg + Ni in the support. Nitrate impregnation was carried out at 45 °C for 48 h. The solution was then slowly evaporated at 100 °C, and the solid was subsequently dried at 120 °C for 15 h. To form the alumina-supported spinel, the following temperature program was applied: heating at 2 °C min^{-1} from 25 to 900 °C (8 h) in air, heating from 900 to 1000 °C at 1 °C min^{-1} (1.5 h) in air, and a plateau at 1000 °C for 15 h in air. Rhodium catalysts (∼0.2 wt% Rh) were prepared by wet impregnation of aqueous solution of rhodium

nitrate at 45 °C, slow evaporation at 100 °C, and drying at 120 °C. The catalysts were finally calcined at 700 °C to stabilize the solid before the reaction. The nomenclature of the first series of catalysts is as follows: N-Rh/1-Mg_xAl, where N is for nitrate and 1 is for the first series. For instance, N-Rh/1-$Mg_{0.75}$Al is the 0.2% Rh ex-nitrate deposited on the $Mg_{0.75}Ni_{0.25}Al_2O_4/Al_2O_3$ support.

The second series of catalysts was prepared over a nickel-free oxide, $MgAl_2O_4/Al_2O_3$. For better control of the acidity of the support, Mg was introduced on alumina as magnesium acetate. Moreover, no aluminum was added, and the spinel was formed via a solid–solid reaction between magnesium oxide (ex-acetate) and the γ-alumina bead. The same temperature program was used as for the first series. This support was impregnated with rhodium nitrate (N-Rh/2-MgAl), rhodium acetate (A-Rh/2-MgAl), or rhodium chloride (C-Rh/2-MgAl). Whereas the impregnation with N-Rh and A-Rh was rather difficult and was restricted to 0.2–0.4 wt% Rh, impregnation of C-Rh was easier, and a rhodium loading of almost 1 wt% could be obtained. The rhodium chloride precursor was selected to vary the Rh loading between 0.2 and 1 wt%.

2.2. Characterization

BET area and pore size distribution were measured in a Flowsorb II apparatus (Micromeritics).

X-ray diffraction analysis was carried out in a Siemens D5005 diffractometer, equipped with a Cu anode (λ = 0.15406 nm). Diffractograms were recorded in the 15°–75° range of 2θ, with a step of 0.04° and a dwell time of 6 s. Phases present in the samples were identified by comparison with ICDD files.

The catalyst morphology was characterized with a 5600 LV Jeol SEM, equipped with a Everhart–Thornley detector for secondary electron analysis and a Centaurus (KE Development, Cambridge) detector for back-diffused electron analysis. The latter detector is especially well-adapted to increase the chemical contrast between light and heavy elements. The microscope was also equipped with an INCA 300 Oxford Instruments system for EDX analysis.

Metal accessibility was measured in a home-made chromatographic apparatus [41,63]. The catalyst sample (typically 500 mg) was reduced in flowing H_2 (30 $cm^3\,min^{-1}$) at 500 °C, outgassed in ultrapure Ar at 500 °C for 1 h, and cooled to room temperature (RT). Pulses of H_2 (0.250 cm^3) were injected every other minute up to saturation (HC_1). A new series of H_2 pulses was injected over the sample, after 10 min of purging under pure Ar, to determine the reversible part of the chemisorbed hydrogen (HC_2). The irreversible part was taken as $HC = HC_1 - HC_2$. Oxygen titration of the chemisorbed hydrogen (OT) and hydrogen titration of the chemisorbed oxygen (HT) were successively carried out, at 25 °C for OT and 60 °C for HT. Oxygen is more strongly bounded on Rh than on Pt, and the HT measurement temperature was adjusted for a complete titration [41]. The stoichiometries for the chemisorptions and titrations were 1:2:4 for HC/OT/HT. On the basis of an equidistribution of the ⟨100⟩, ⟨110⟩, and ⟨111⟩ faces, the molar surface area of rhodium would be 45,700 $m^2\,mol^{-1}$. In the classical hypothesis of cubic particles with one face in contact with the support (five faces exposed to the gases), the metal particle size can be calculated as

$$d\ (\mathrm{nm}) = \frac{91}{D},$$

where D is the metal accessibility as a percentage.

Acidic and basic properties were characterized by means of the activity in the dimethyl-3,3-but-1-ene (DM33B1) isomerization (acidity) and the CO_2 chemisorption (basicity) [64,65]. DM33B1 isomerization was carried out at temperatures ranging from 200 to 400 °C on the samples (typically 0.1 g) previously calcined in situ in air (30 $cm^3\,min^{-1}$) at 450 °C and cooled to the reaction temperature under N_2. DM33B1 was injected by means of a saturator maintained at 0 °C (DM33B1 partial pressure 20.9 kPa) under flowing nitrogen (30 $cm^3\,min^{-1}$). Reactant and products (dimethyl-2,3-but-2-ene, DM23B2 and dimethyl-2,3-but-1-ene, DM23B1) were analyzed on line by GC on a squalane column (100 m × 0.25 mm) maintained at 50 °C. Carbon dioxide chemisorption was carried out in a chromatographic apparatus similar to the one described for hydrogen chemisorption and titrations. The sample (0.1 g) was previously oxidized in situ at 450 °C and then cooled to RT under flowing He (30 $cm^3\,min^{-1}$). CO_2 pulses (0.25 cm^3) were injected up to the saturation point.

Some catalysts (second series) were also characterized by FTIR of adsorbed lutidine (Nexus, Nicolet). The sample was crushed to obtain a very fine powder and then pressed (120 $kg\,cm^{-2}$) to form a self-supported pellet about 16 mm in diameter (∼20 mg). The sample was outgassed under vacuum (10^{-5} mbar) at 600 °C (1 h) and cooled to RT. Lutidine was adsorbed at 25 °C. Because of the difficulties encountered in pelletizing the Rh/spinel catalysts, some of them were investigated by DRIFT, with attention focused on the 3000–4000 cm^{-1} spectral region. For DRIFT measurements, the samples (25 mg) were simply outgassed under pure Ar at 600 °C before the spectra were recorded at 25 °C.

2.3. Ethanol steam reforming reaction

Ethanol steam reforming was carried out at 1 or 11 bar. Anhydrous ethanol (Rectapur Prolabo) was used. The steam reforming reaction was carried out in a flow reactor (L = 550 mm; $\varnothing_{int}$ = 12.5 mm) made of refractory steel (TP 310 Z15CNS25). The ethanol–water mixture was injected with syringes (1 bar) or a pump (11 bar). The mixture was preheated at 120 °C before entering the reactor. The catalyst sample (typically 500 mg) was diluted in carborundum (2.5 g), with about the same particle size. It was placed in the middle of the reactor tube near the temperature controller thermocouple. Another thermocouple was inserted in

the catalyst bed and used to measure both the external temperature of the catalyst and the axial gradient in the bed. Void fractions of the reactor were packed with carborundum. It was found that a temperature drop of less than 5 °C occurred upon reactant injection. These are the stabilized temperatures that are given in the tables. The reactor can be fed with pure H_2 (catalyst reduction) or pure nitrogen for air purging. The reaction gases were passed through a condenser at +0.5 °C to collect the nonreacted water and ethanol, acetaldehyde, and traces of acetone, acetic acid, and propanoic acid. Noncondensable gases at +0.5 °C (H_2, CO, CO_2, CH_4, ethylene, ethane) were analyzed on line by GC (TCD1 carrier gas: N_2 to detect H_2; TCD2 carrier gas: H_2 to detect CO_x and CH_4, FID to detect the hydrocarbons). CO_x concentrations were also controlled with the use of IR analyzers, especially at low CO_x concentrations. The condensed liquids were analyzed by HPLC on an Aminex HPX-87H column, combining a refractometer and a UV diode array detector. Before each test, the catalyst sample was reduced under H_2 (50 $cm^3\,min^{-1}$) at 500 °C and heated at 10 °C min^{-1} to the reaction temperature under N_2 (50 $cm^3\,min^{-1}$). The gas hourly space velocity (GHSV) is defined as

$$\text{GHSV}\ (\text{h}^{-1}) = \frac{D_g \times \rho_c}{m},$$

where D_g is the reactant gas flow rate (ethanol + steam) in $cm^3\,h^{-1}$ (25 °C, 1 atm), ρ_c is the apparent catalyst density ($g\,cm^{-3}$), and m is the catalyst weight (g).

The residence time in the catalyst bed was

$$\delta\ (\text{ms}) = \frac{3.6 \times 10^6}{\text{GHSV}(\text{h}^{-1})}.$$

If n_X^{in} and n_X^{out} are, respectively, the molar flow rates of product X at the inlet and outlet of the reactor, the catalyst reactivity is characterized by

- the dry gas composition (in vol%);
- the ethanol conversion:

$$X_{EtOH} = \frac{n_{EtOH}^{in} - n_{EtOH}^{out}}{n_{EtOH}^{in}} \times 100;$$

- the hydrogen yield (mole of H_2 per mole of converted EtOH):

$$Y_{H_2} = \frac{n_{H_2}^{out}}{n_{EtOH}^{in} - n_{EtOH}^{out}};$$

- the selectivity in C-products:

$$S_X = \frac{n_X^{out}}{\chi\,(n_{EtOH}^{in} - n_{EtOH}^{out})};$$

where χ is the stoichiometry factor (2 for C_1 and 1 for C_2 compounds).

To give an efficiency of the overall process, including steam reforming and WGS, a theoretical hydrogen yield is also calculated (supposing a total conversion of CO into $H_2 + CO_2$ by WGS):

$$Y_{H_{2th}} = Y_{H_2} \times \frac{n_{H_2}^{out} + n_{CO}^{out}}{n_{H_2}^{out}}.$$

3. Results

3.1. Physical and chemical properties of the first series of supports and catalysts

BET surface areas and textural properties of the first series of supports are listed in Table 1. Also listed in Table 1 are the characteristics of the starting γ-alumina (denoted Al). All supported spinels show similar textural properties. In spite of the high-temperature treatments (1000 °C), spinels maintained relatively high BET surface areas of about 100 $m^2\,g^{-1}$. Compared with the initial γ-alumina, the pore volume of the spinels decreased by 41 ± 2%, and the mean pore size increased by 27 ± 2%. There were virtually no micropores (<2 nm) in these supports, and the mass transport in the core of the support was facilitated.

The acidic and basic properties of the solids examined in the DM33B1 isomerization at 300 °C and by CO_2 chemisorption at 25 °C are summarized in Fig. 1. The corresponding values for the starting γ-alumina were, respectively, 245 µmol h^{-1} m^{-2} for the DM33B1 isomerization and 0.30 µmol m^{-2} for the CO_2 chemisorption. Acidity decreases with x, that is, from pure $NiAl_2O_4$ to pure $MgAl_2O_4$. However, all of the supported spinels were significantly less acidic than the alumina itself. These results showed that (i) $Mg_xNi_{1-x}Al_2O_3$ supports do not possess strong acidic sites and (ii) the spinel oxide forms a rather continuous layer at the alumina bead surface. On the other hand, the support basicity increases with x. Furthermore, the basicity of the supported spinels is stronger than that of the starting γ-alumina, whatever the Mg content.

The characteristics of the Rh/$Mg_xNi_{1-x}Al_2O_3$/Al_2O_3 catalysts are listed in Table 2. The characteristics of a 0.2% Rh catalyst directly deposited on the starting alumina (N-Rh/Al) are also listed in Table 2. Moderate differences were found between the catalysts. The metal impregnation decreased the BET surface area of the support only slightly

Table 1
Nomenclature and characteristics of the $Mg_xNi_{1-x}Al_2O_4$/Al_2O_3 supports (first series)

Support	BET surface area ($m^2\,g^{-1}$)	Pore volume ($cm^3\,g^{-1}$)	Micropore volume ($cm^3\,g^{-1}$)	Average pore size (nm)
Al	200	0.477	0.009	8.6
1-Mg_1Al	103	0.290	0.008	11.1
1-$Mg_{0.75}$Al	103	0.292	0.008	11.0
1-$Mg_{0.5}$Al	101	0.288	0.007	11.1
1-$Mg_{0.25}$Al	102	0.286	0.008	10.8
1-Mg_0Al	96	0.272	0.005	10.9

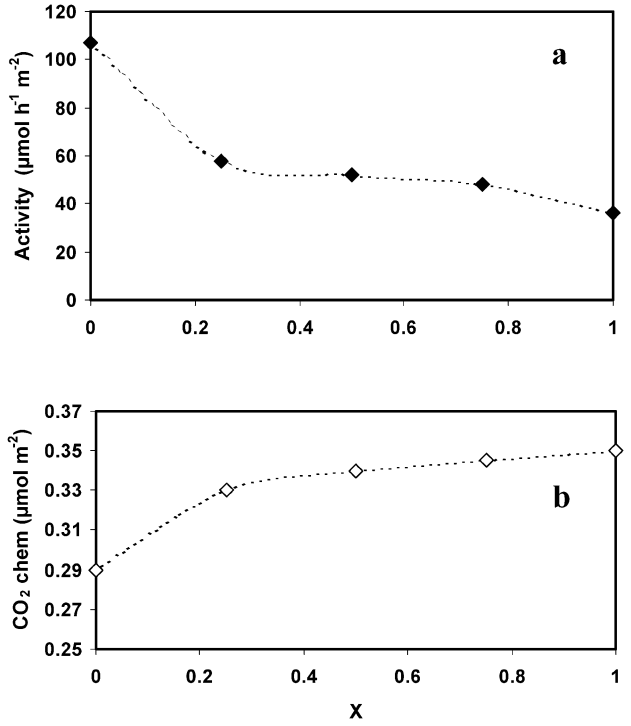

Fig. 1. Acidic and basic properties of the $Mg_xNi_{1-x}Al_2O_3$ spinel oxides supported on γ-alumina (first series): (a) activity in the DM33B1 isomerization at 300 °C; (b) CO_2 chemisorption at 25 °C.

Table 2
Nomenclature and characteristics of the $Rh/Mg_xNi_{1-x}Al_2O_4/Al_2O_3$ catalysts (first series)

Catalysts	BET surface area ($m^2\ g^{-1}$)	Metal loading (wt%)	Metal accessibility (%)	Metal surface area ($m^2_{Rhs}\ g^{-1}$)	Average particle diameter (nm)
N-Rh/Al	190	0.20	40	0.355	2.3
N-Rh/1-Mg_1Al	104	0.16	45	0.319	2.0
N-Rh/1-$Mg_{0.75}$Al	96	0.17	38	0.287	2.4
N-Rh/1-$Mg_{0.50}$Al	93	0.12	40	0.213	2.3
N-Rh/1-$Mg_{0.25}$Al	95	0.20	48	0.426	1.9
N-Rh/1-Mg_0Al	89	0.10	42	0.186	2.2

(−8% max). In every case, the metal accessibility was close to 40%, and the mean rhodium particle size was between 1.9 and 2.4 nm.

3.2. Activity of the first series of catalysts (1 and 11 bar)

The catalyst performances in the ethanol steam reforming at 700 °C and $R = 4$ are listed in Table 3 (1 bar) and Table 4 (11 bar). A GHSV of 13400 h^{-1} corresponds to a residence time of 268 ms in the catalyst bed (500 mg). The figures listed in Tables 3 and 4 represent the mean values obtained after 7 to 24 h on stream, except for N-Rh/1-Mg_0Al at 1 bar

Table 3
Ethanol steam reforming at atmospheric pressure ($T = 700$ °C, GHSV = 13400 h^{-1}, $R = 4$)

	Dry gas composition (%)						X_{EtOH} (%)	H_2 yield (mol mol^{-1})	H_2 yield with WGS[a]
	H_2	CO_2	CO	CH_4	$C_2H_4 + C_2H_6$	CH_3CHO			
Equilibrium composition	70.0	12.5	16.7	0.8	0	0	100	4.7	5.82
SiC only	39.8	0.6	20.0	19.2	12.7	7.7	70.8	0.59	0.88
Al_2O_3 only	43.2	0.7	21.9	20.7	13.4	8.7	71.0	0.42	0.63
N-Rh/1-Mg_1Al	68.9	14.6	13.5	3.0	0	0.1	100	4.41	5.27
N-Rh/1-$Mg_{0.75}$Al	65.1	8.9	20.5	4.8	0.6	0.2	96	3.61	4.75
N-Rh/1-$Mg_{0.50}$Al	66.1	12.5	17.0	4.0	0.3	0.1	100	3.90	4.91
N-Rh/1-$Mg_{0.25}$Al	70.2	13.6	13.4	2.7	0	0.1	100	4.68	5.58
N-Rh/1-Mg_0Al[b]	67.2	13.1	14.4	4.1	0.9	0.3	94	3.95	4.80

[a] Initial activity.
[b] Theoretical values supposing a total conversion of $CO + H_2O$ into $H_2 + CO_2$.

Table 4
Ethanol steam reforming at 11 bar ($T = 700$ °C, GHSV = 13400 h^{-1}, $R = 4$)

	Dry gas composition (%)						X_{EtOH} (%)	H_2 yield (mol mol^{-1})	H_2 yield with WGS[a]
	H_2	CO_2	CO	CH_4	$C_2H_4 + C_2H_6$	CH_3CHO			
Equilibrium composition	58.2	17.1	10.6	14.1	0	0	100	2.79	3.30
SiC only	35.5	4.4	27.2	25.8	6.6	0.4	98	0.95	1.67
Al_2O_3 only	29.2	1.8	31.2	28.8	9.0	0.3	99	0.71	1.47
N-Rh/Al	55.6	16.2	12.7	15.3	0.2	0	99	2.50	3.07
N-Rh/1-Mg_1Al	57.8	17.5	10.6	14.0	0.1	0.1	100	2.74	3.25
N-Rh/1-$Mg_{0.75}$Al	57.6	17.7	10.1	14.6	0	0	100	2.64	3.11
N-Rh/1-$Mg_{0.25}$Al[b]	56.7	19.4	8.8	15.0	0	0	100	2.61	3.02

[a] Initial activity.
[b] Theoretical values supposing a total conversion of $CO + H_2O$ into $H_2 + CO_2$.

and N-Rh/1-$Mg_{0.25}Al$ at 11 bar. In fact, these catalysts were not stable enough over a 1-day test, and the activities we reported correspond to the "initial" activities after 2–7 h on stream. Moreover, the very poor stability of N-Rh/1-Mg_0Al at 11 bar did not even allow us to measure the activity over 7 h.

At atmospheric pressure and 700 °C, SiC or α-Al_2O_3 (2.5 g), used as dilutants, could convert up to 71% of the ethanol. Nevertheless, the conversion was essentially due to the ethanol cracking, the dehydration, and the dehydrogenation, with major production of CO, methane, C_2 hydrocarbons, and acetaldehyde. The hydrogen yield was limited, well below the thermodynamic yield. Moreover, a relatively large amount of coke was deposited on the diluant and the reactor walls. Blank experiments (empty reactor) were also carried out. Ethanol conversions are slightly lower than those obtained with alumina or SiC. Acetaldehyde/C_2 hydrocarbons ratios were higher, suggesting that alumina and SiC promoted the dehydration reaction. The catalysts deposited on 1-Mg_1Al and 1-$Mg_{0.25}Al$ showed very promising performances at 1 bar, and, compared with the other catalysts, virtually no ethylene, very little acetaldehyde, and significantly less methane were produced, even though equilibrium was not reached. Methane can be produced by ethanol cracking or CO hydrogenation and then is reformed into H_2 and CO_x. The fact that the methane level is above equilibrium suggests that CH_4 reforming is not very rapid at 700 °C, 1 atm. Although one could argue about the differences between these catalysts, especially based on the metal loading and accessibility, such differences still appear to be significant. The theoretical hydrogen yield (including WGS) could reach 5.58 mol $\text{mol}^{-1}_{C_2H_5OH}$ on the most active catalyst.

When the reaction is carried out under 11 bar, SiC and α-Al_2O_3 are even more active (98–99% conversion). Again, Y_{H_2} is very poor because of the very high reaction selectivity in CO, methane, and ethylene. All of the tested spinel-supported catalysts showed performances close to equilibrium. One can see that increasing the pressure decreases the thermodynamic hydrogen yield, essentially because the production of methane is strongly favored. N-Rh/1-Mg_1Al is the most active among the three Mg_x spinel-supported samples. All spinel-supported catalysts exhibit better performances than Rh/Al_2O_3. This catalyst could not convert all of the ethanol injected and produces more CO, methane, and ethylene than the supported spinel catalysts.

The stability of the N-Rh/1-Mg_1Al catalyst was tested over 75 h on stream, first at atmospheric pressure and then at 11 bar (Fig. 2). This catalyst showed a very good stability. Except for a short period after the pressure increase, the ethanol conversion was total. The gas composition is apparently stable. However, it can be seen that the CO concentration slowly increased with time at the expense of CH_4 and CO_2. Moreover, more and more ethylene was formed throughout the test, indicating a very progressive modification of the catalyst. In fact, some coke covered the entire catalyst (visual evidence). Of course, such a coke invasion in the reactor could affect the long-term stability of the catalyst and cause the reactor operation to rapidly deteriorate. Since the production of ethylene derives from the ethanol dehydration reaction, better performance (activity and stability) would be expected from a better control of the catalyst surface acidity.

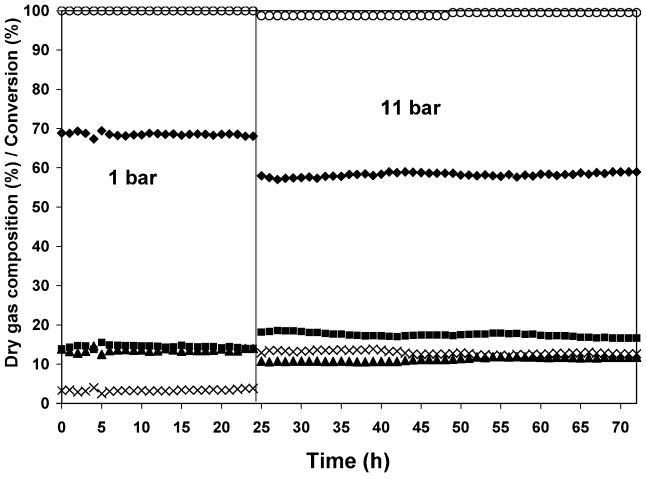

Fig. 2. Stability test over N-Rh/1-Mg_1Al at $P = 1$ and 11 bar, $T = 700$ °C, GHSV = 13,400 h^{-1} and water:ethanol molar ratio $R = 4$: (○) ethanol conversion; (◆) H_2; (■) CO_2; (▲) CO; (◇) CH_4. Other gases (acetaldehyde + ethylene + ethane) <1%.

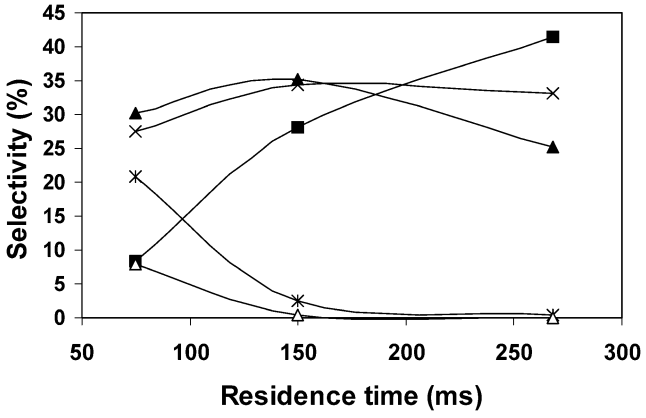

Fig. 3. Influence of the residence time on the C-products distribution upon reaction at $T = 700$ °C, $P = 11$ bar and water:ethanol molar ratio = 4: (■) CO_2, (▲) CO, (×) CH_4, (∗) $C_2H_4 + C_2H_6$, (△) CH_3CHO.

The product evolution was also investigated at lower residence times (δ) over N-Rh/1-Mg_1Al. The results are reported in Fig. 3. Acetaldehyde and C_2 hydrocarbons were clearly identified as the primary products, and CO_2 appears to be a secondary product. Consequently, one can conclude that ethanol dehydration and dehydrogenation occur first, before the steam reforming reaction itself.

The evolutions for CO and CH_4 were more complex. As the contact time decreased, the selectivities passed through some kind of a maximum but still remained quite high at the lowest residence time. This result suggests that there is a direct route for the CO and CH_4 formation, independent of the steam reforming and the successive interconversion reac-

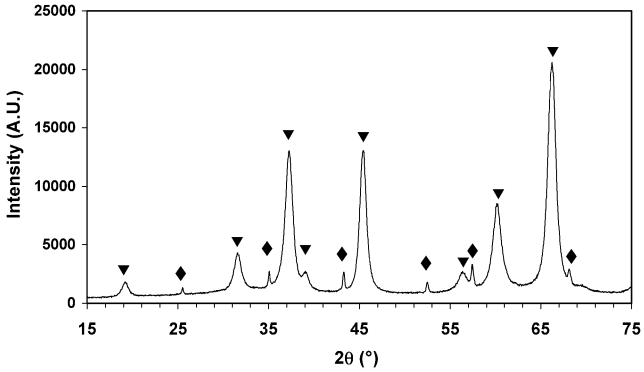

Fig. 4. X-Ray diffractograms for 2-Mg_1Al supports: (▼) $Mg_{0.388}Al_{2.408}O_4$ (ICDD n° 76-0306), (◆) α-Al_2O_3 (ICDD n° 83-2080).

Table 5
Nomenclature and characteristics of the $MgAl_2O_4/Al_2O_3$ supports

Support	Mg loading (wt%)	BET surface area ($m^2\,g^{-1}$)	Pore volume ($cm^3\,g^{-1}$)	Micropore volume ($cm^3\,g^{-1}$)	Average pore size (nm)
Al	–	200	0.477	0.009	8.6
1-Mg_1Al	5.0	103	0.290	0.008	11.1
2-Mg_1Al	4.6	94	0.268	0.010	10.8

tions between gases (water gas shift, CO and CO_2 methanation). This independent route could be the ethanol cracking, as mentioned in the Introduction (reaction (7)).

3.3. Physical and chemical characteristics of the $MgAl_2O_4/Al_2O_3$ support (second series)

A new $MgAl_2O_4/Al_2O_3$ support (denoted 2-Mg_1Al) was prepared with the aim of minimizing the surface acidity. The X-ray diffractogram of this support confirmed that the solid-state reaction of magnesium oxide with alumina is total (Fig. 4): no trace of MgO or $Mg(OH)_2$ could be detected. XRD lines of the spinel are very close to $Mg_{0.388}Al_{2.408}O_4$ (ICDD file no. 76-0306), indicating some possible distortions in the spinel structure. Minute amounts of α-Al_2O_3 (ICDD file no. 83-2080) were also detected in the support, and the unreacted fraction of the alumina (core) is likely to form δ or θ-Al_2O_3.

The average spinel crystal size derived from the Debye-Scherrer equation, based on the most intense peaks (⟨311⟩ at 37.3° and ⟨400⟩ at 45.5°), is 8.7 nm, whereas the average size of the α-Al_2O_3 crystallite is 41 nm. A comparison of the textural properties of 2-Mg_1Al compared with 1-Mg_1Al and Al shows that the two supported spinels have very similar porosities and BET surface areas (Table 5). Although a small decrease in the BET surface area and the pore volume is recorded for 2-Mg_1Al (about 8% with respect to 1-Mg_1Al), the mean pore size remains very close for the two supports (≈11 nm), and a fast diffusion of the gases within the pores is still possible.

SEM observations coupled with the Mg local analysis were used to precisely determine the morphology of the Mg-spinel deposit (Fig. 5). In the SEM pictures, the core-shell structure of the beads can be clearly observed. The outer part of the bead (thickness ≈160–200 μm) was slightly darker than the inner part, indicating that the local composition in the shell was different from the core. EDS analysis revealed a higher concentration in Mg at the bead periphery.

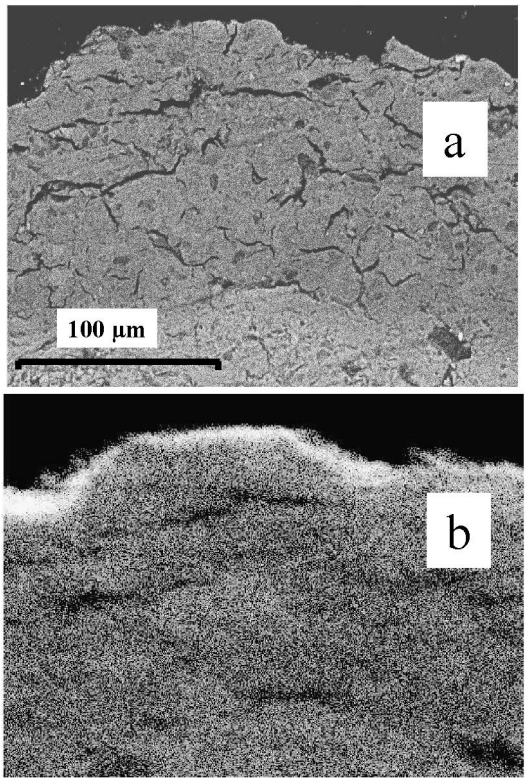

Fig. 5. SEM image of the 2-Mg_1Al support (a) and local analysis of Mg (b). The intensity of the white dots is proportional to the Mg concentration.

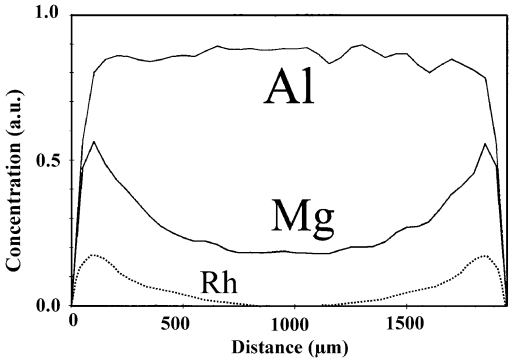

Fig. 6. Microprobe analysis of Al and Mg along the diameter of a 2-Mg_1Al bead. (···) Rh profile on the same support (C-Rh/2-Mg_1Al).

This result is confirmed by the microprobe analysis of the Al and Mg concentrations across the bead (Fig. 6). Whereas the Al concentration remains logically constant all along the diameter, the profile for Mg is characteristic of an eggshell type of structure, with an outer concentration in Mg almost three times higher than the core concentration.

Table 6
Acidic and basic properties of the Al_2O_3 and $MgAl_2O_4/Al_2O_3$ supports

Support	Activity in DM33B1 isomerization ($\mu mol\ m^{-2}\ h^{-1}$)			Chemisorbed CO_2 ($\mu mol\ m^{-2}$)
	300 °C	350 °C	400 °C	
Al	245	–	–	0.30
1-Mg_1Al	36	66	95	0.35
2-Mg_1Al	34	60	71	0.36

Table 7
Nomenclature and metal dispersion of Rh catalysts (second series)

Catalyst	BET surface area ($m^2\ g^{-1}$)	Loading (wt%)		Metal accessibility (%)	Average particle size (nm)
		Rh	Cl		
C-Rh/Al	193	0.93	0.87	42	2.2
A-Rh/2-Mg_1Al	97	0.37	–	9	10.1
N-Rh/2-MgAl	101	0.20	–	26	3.5
C_1-Rh/2-Mg_1Al	95	0.25	0.15	54	1.7
C_2-Rh/2-Mg_1Al	94	0.35	0.25	51	1.8
C_3-Rh/2-Mg_1Al	95	0.82	0.53	47	1.9

The acidic and basic properties of 2-Mg_1Al were also compared with those of 1-Mg_1Al and γ-Al_2O_3 (Table 6). 2-Mg_1Al appeared to be slightly less acidic than 1-Mg_1Al, with virtually no change in the basic properties. Activation energy for DM33B1 isomerization is significantly lower on 2-Mg_1Al (21 kJ mol^{-1}) compared with 1-Mg_1Al (31 $kJ\ mol^{-1}$). This observation indicates that the second spinel possesses weaker acidic sites compared with the first one.

3.4. Physical and chemical properties of $MgAl_2O_4/Al_2O_3$-supported Rh catalysts (second series)

The textural and chemical characteristics and the metal dispersion for Rh/γ-Al_2O_3 and Rh/$MgAl_2O_4/Al_2O_3$ catalysts are given in Table 7. Impregnation with rhodium acetate is very difficult, and thus a significant part of the rhodium salt was not retained on the support. As a result the metal was not well dispersed, and the mean rhodium particle size was 10.1 nm. With the nitrate precursor, fairly good dispersions were obtained. Finally, with the chloride precursor salt, the rhodium is easily impregnated, and the metal particles size was between 1.7 and 1.9 nm.

Keeping in mind that these catalysts were pretreated at 700 °C in air before the reduction, it can be concluded that the chloride precursor led to stable catalysts when supported on spinel oxides. The rhodium impregnation did not change the BET surface area of 2-Mg_1Al. The surface area of the resulting catalysts may have even been slightly higher compared with the support (nitrate precursor). Microprobe analysis showed that the Rh and Mg profiles were very similar and that both elements were mainly localized at the bead periphery, which prevented heat and mass transfer limitations inside the catalyst beads (Fig. 6). This observation tends to prove that Rh is more likely to be impregnated on the spinel and not on alumina.

Table 8
Acidic and basic properties of the $MgAl_2O_4/Al_2O_3$-supported Rh catalysts (second series)

Catalyst	DM33B1 isomerization		CO_2 chemisorption
	Reaction temperature (°C)	Activity ($\mu mol\ m^{-2}\ h^{-1}$)	CO_2 uptake at 25 °C ($\mu mol\ m^{-2}$)
A-Rh/2-Mg_1Al	200	1	0.38
	250	3	
	300	4	
C_3-Rh/2-Mg_1Al	200	8	0.16
	250	22	
	300	62	
N-Rh/2-Mg_1Al	200	15	0.50
	250	134	
	300	600	

Performances in the DM33B1 isomerization for the second series of catalysts are listed in Table 8. Rhodium acetate led to the less acidic catalyst (4 $\mu mol\ m^{-2}\ h^{-1}$ at 300 °C), which was much less acidic than the starting support (34 $\mu mol\ m^{-2}\ h^{-1}$ at 300 °C). Chlorine ions slightly increased the overall acidity of the catalysts, whereas the impregnation with the nitrate precursor created much stronger acidic sites at the spinel surface, although nitrate ions were completely decomposed during the catalyst pretreatment. Most likely nitrate ions could lead to the dissolution–precipitation of the support upon impregnation, especially the Al ions, which may have been responsible for the creation of such strong acid sites.

CO_2 uptakes at 25 °C are also listed in Table 8. The catalyst prepared with the chlorinated precursor lost about 50% of the basic sites upon Rh impregnation. Cl^- ions slightly increased the global acidity of the solid but strongly decreased the basicity. The acetate precursor did not modify the basicity (0.38 vs. 0.36 $\mu mol_{CO_2}\ m^{-2}$), whereas, surprisingly, the nitrate salt increased the basicity. As indicated above, the nitrates would affect the surface state of the support and increase both acidic and basic sites.

Furthermore, FTIR spectra for the adsorbed 2,6-lutidine (2,6-dimethylpyridine) at ambient temperature are shown in Fig. 7. The adsorbed lutidine molecule normally gives bands at 1580 and 1610 cm^{-1}, characteristic of Lewis acid sites, and a doublet at 1628–1645 cm^{-1}, corresponding to the Brønsted acid sites [66–71]. The band at 1610 cm^{-1} appears in Fig. 7 as a doublet with one component at 1615 cm^{-1} ascribed to strong Lewis acid sites and a second one at 1605 cm^{-1} ascribed to the weaker Lewis acid sites or the 2,6-lutidine adsorbed via hydrogen bond [71]. All three catalysts investigated by FTIR exhibited a band at 1615 cm^{-1}. However, the C_3-Rh/2-Mg_1Al catalyst (spectrum c) apparently had the highest number of Lewis acid sites. In fact, it appeared that the chlorinated rhodium precursor had a definite promoter effect on the Lewis acidity of the Mg–Al spinel oxide, which was much more pronounced compared

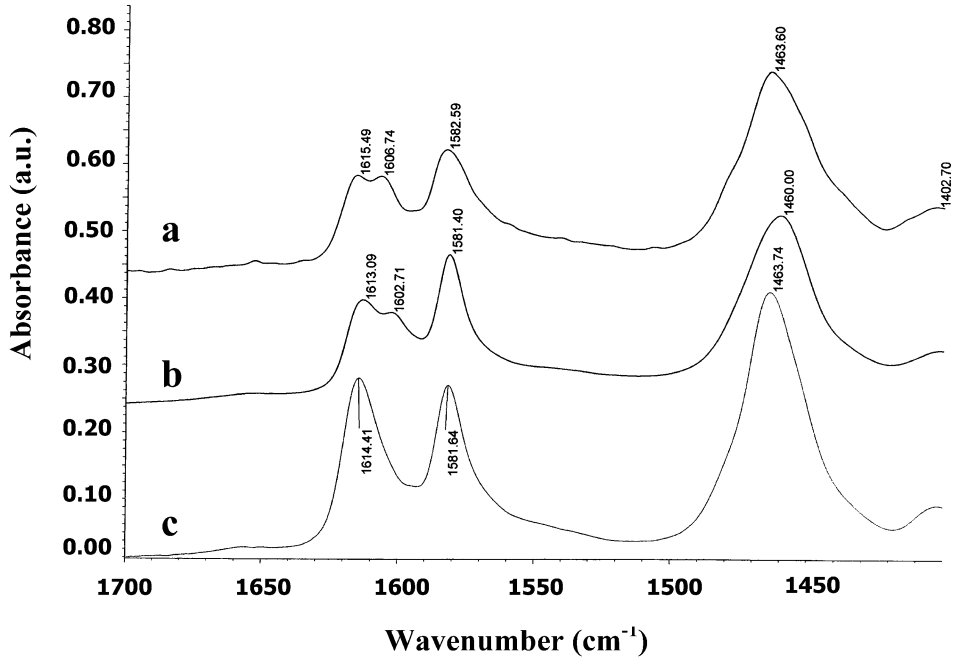

Fig. 7. FTIR spectra of adsorbed lutidine over C-Rh/Al (a), A-Rh/2-Mg_1Al (b) and C_3-Rh/2-Mg_1Al (c).

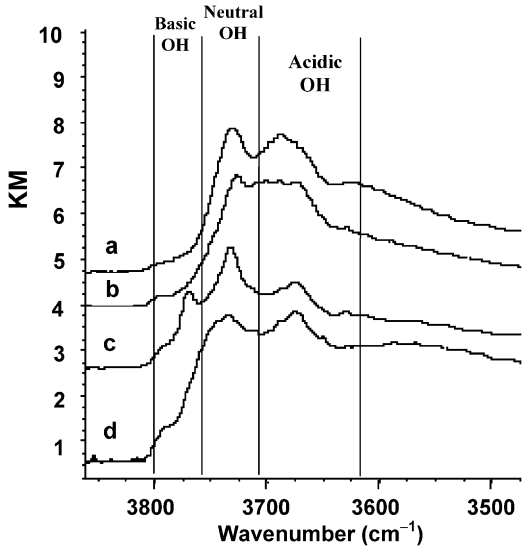

Fig. 8. DRIFT spectra of C-Rh/Al (a), C_3-Rh/2-Mg_1Al (b), A-Rh/2-Mg_1Al (c) and N-Rh/2-Mg_1Al (d).

with the alumina itself. Bands at 1628–1645 cm^{-1} are virtually absent, which means that Brønsted sites are were weak and were not titrated by 2,6-lutidine.

DRIFT spectra, centered in the OH region around 3800–3500 cm^{-1}, are shown in Fig. 8. The broad band characteristic of OH groups can be divided into three spectral domains according to the classification by Knözinger and Ratnasamy [72]:

(i) 3800–3760 cm^{-1}: basic OH groups with a band at 3772 cm^{-1} characteristic of Al^{VI}–OH groups (located on lateral planes and kinks) and another band at 3794 cm^{-1} representative of Al^{IV}–OH groups (located on basal planes).

(ii) 3760–3710 cm^{-1}: neutral OH groups with a band at 3745 cm^{-1} corresponding to neutral or slightly basic Al–OH groups and another band centered at 3730 cm^{-1} indicative of neutral or slightly acidic Al–OH functional groups.

(iii) 3710–3610 cm^{-1}: acidic OH group with a typical band at 3685 cm^{-1} characteristic of type III Al^{VI}–OH groups.

Table 9
Relative intensities of the bands characteristic for basic and acidic OH groups in the DRIFT spectra for Rh/$MgAl_2O_4$/Al_2O_3 catalysts (second series)

Catalyst	Basic OH/neutral OH	Acidic OH/neutral OH
C-Rh/Al	0.11	1.32
C-Rh/2-Mg_1Al	0.15	1.41
A-Rh/2-Mg_1Al	0.40	0.96
N-Rh/2-Mg_1Al	0.31	1.18

The two bands characteristic of neutral OH groups at 3745 and 3730 cm^{-1}, respectively, cannot be distinguished in the DRIFT spectra of Fig. 8. However, the intensity is virtually constant and might be used as a reference to follow the evolution of the concentration in basic and acidic OH groups on the different catalysts (Table 9).

The ex-acetate catalyst is clearly the most basic and the less acidic material. On the corresponding spectrum, a relatively intense band is observed around 3770 cm^{-1}, characteristic of OH groups on surface defects. Ex-chloride samples possess the greatest number of acidic OH groups and virtually no basic sites. The highest acidity of the C sam-

Table 10
Ethanol steam reforming over the catalysts of the second series ($T = 700\,°C$, $P = 11$ bar, GHSV = 13400 h^{-1}, $R = 4$)

	Dry gas composition (%)						X_{EtOH} (%)	H_2 yield (mol mol^{-1})	H_2 yield with WGS[a]
	H_2	CO_2	CO	CH_4	$C_2H_4 + C_2H_6$	CH_3CHO			
Equilibrium composition	58.2	17.1	10.6	14.1	0	0	100	2.79	3.30
C-Rh/Al	59.1	17.3	10.5	12.7	0.3	0	99	2.76	3.25
A-Rh/2-Mg_1Al	58.6	15.8	11.9	13.3	0.3	0	100	2.82	3.39
C_1-Rh/2-Mg_1Al[b]	52.7	14.5	15.1	16.8	0.9	0	100	2.15	2.77
C_2-Rh/2-Mg_1Al	53.6	16.1	14.1	15.6	0.6	0	100	2.27	2.87
C_3-Rh/2-Mg_1Al	58.6	16.7	10.9	13.6	0.2	0	100	2.83	3.36
N-Rh/2-Mg_1Al[b]	53.1	13.5	15.1	17.4	0.9	0	99	2.09	2.68

[a] Average activity during the first 2 h.
[b] Theoretical values supposing a total conversion of $CO + H_2O$ into $H_2 + CO_2$.

ples is confirmed. However, it should be kept in mind that the catalyst can be progressively dechlorinated in the course of the steam reforming reaction, which tends to decrease the acidity because of the use of Rh chloride as a metal precursor.

3.5. Activity of the second series of catalysts (11 bar)

The catalysts were tested in the ethanol steam reforming at 700 °C and a total pressure of 11 bar. The mean values, collected after 2 to 24 h on stream, are listed in Table 10.

The Cl-Rh/Al_2O_3 catalyst showed a good activity for H_2 production. However, despite the high Rh loading, the ethanol conversion was not total. Furthermore, the carbon balance was relatively low (96%), indicating a continuous carbon formation on the catalyst surface with a slight but continuous deactivation over a longer time on stream. Unfortunately, it was not possible to impregnate the support with Rh nitrate, without any loss of Rh salt, beyond 0.2 wt%. The resulting catalyst had a relatively poor H_2 yield. Moreover, ethanol conversion was not 100%, and the catalyst was not stable.

Impregnation with Rh chloride is much easier and gives well-dispersed catalysts. Increasing the Rh loading from 0.25 to 0.82 wt% brought the gas distribution closer and closer to the equilibrium composition. The yields in H_2 and CO_2 increased and the CO, CH_4, and C_2 hydrocarbons decreased. The C_3-Rh/2-Mg_1Al catalyst (0.82% Rh) led to the highest H_2 yield, 2.82 $mol_{H_2}\,mol^{-1}_{Ethanol}$ or 2.22 $g_{H_2}\,h^{-1}\,g^{-1}_{cat}$. No apparent deactivation was observed over 24 h. Interesting performances were obtained with the ex-acetate catalyst. The H_2 production rate was high in spite of the relatively low Rh content and the poor Rh dispersion. The unique acidic and basic properties of this catalyst (significant basicity and very weak acidity) could explain such results. As a rule, it appeared that under the chosen conditions, a catalyst with as little as 0.4 wt% Rh may achieve 100% ethanol conversion with a production rate of 2.20 $g_{H_2}\,h^{-1}\,g^{-1}_{cat}$ or 550 $g_{H_2}\,h^{-1}\,g^{-1}_{Rh}$, that is, a thermal power of 18.3 kW per gram of rhodium.

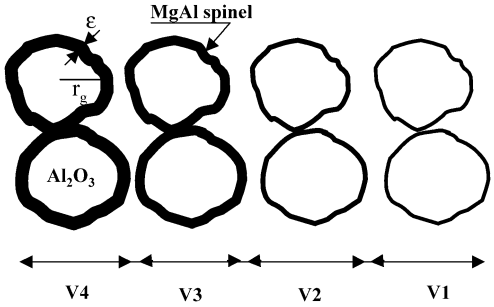

Fig. 9. Schematic picture of the morphology of the $MgAl_2O_4/Al_2O_3$ support (second series).

4. Discussion

4.1. Support morphology

Looking at all the information concerning the $MgAl_2O_4/Al_2O_3$ support (second series) collected in Table 5 and Figs. 4–6, one might obtain a relatively precise picture of the support morphology. Such a support consists of beads about 2 mm in diameter with a decrease in the Mg content from the periphery to the center of the bead (Fig. 6). The global Mg content in the support was 4.60 wt%, and we could derive the Mg profile in the bead. The volume of each bead, assimilated to a sphere of radius r_g, was divided into four elementary volumes: the inner sphere of radius $r/4$ and three spherical shells between $r/4$ and $r/2$, $r/2$ and $3r/4$, and $3r/4$ and r. The four volumes are respectively denoted V_1, V_2, V_3, and V_4 from the inner to the outer part of the bead. Calculations, detailed in the Appendix A, show that the mean Mg contents were 2.21% in V_1, 2.51% in V_2, 3.62% in V_3, and 5.56% in V_4. Moreover, if one assumes that (i) the bead consists of alumina grains and (ii) the MgAl-spinel forms a regular shell of thickness ε around each alumina grain (radius r_g), the ε/r_g ratio would be 3.3% in V_1, 3.8% in V_2, 5.7% in V_3, and 9.5% in V_4 (Fig. 9). Going from the core of the bead to the periphery, the spinel layer covering the alumina grain becomes thicker and thicker.

The size of the alumina grain defined above is not known. However, one could imagine it is close to the size of the α-Al_2O_3 crystallites detected by XRD. In fact, the alumina

grains could form by crystallization of the polycrystalline transition alumina grains into single crystals of α-Al_2O_3. However, from the outer volume V_4, which contains the major part of the magnesium, the calculated ε/r_g ratio (9.5%) is much smaller than the observed ratio between the spinel crystallite size (8.7 nm) and the crystallite size for α-Al_2O_3 (41 nm, i.e., $r_g = 20.5$ nm) as measured from XRD. Two hypotheses may explain such a discrepancy: (i) the size of the alumina grains in the bead is much larger than the α-Al_2O_3 crystals formed upon high-temperature treatment or (ii) the spinel composition is not $MgAl_2O_4$ but closer to $Mg_{0.388}Al_{2.408}O_4$, as identified by XRD (Fig. 4). To check the second hypothesis, if one considers the new stoichiometry ratio $y = Al/(2Mg) = 3$, the calculated ε/r_g ratio becomes 10.7% in V_1, 12.5% in V_2, 19.8% in V_3, and 39.1% in V_4 (see Appendix A). In that case, the calculated ε/r_g ratio in V_4 would be very close to the ε/r_g ratio derived from XRD (42.4%). Consequently, the second hypothesis should be preferred.

In summary, the support beads would consist of agglomerated alumina grains (about 40 nm in size) coated with the MgAl spinel (8–9 nm in size) with an excess in Al ions.

4.2. Role of the acidic and basic properties of the catalyst

Ethanol is very rapidly dehydrated and dehydrogenated on the catalysts under study, and ethylene and acetaldehyde appeared to be primary products in the ethanol steam reforming reaction (Fig. 3).

Alcohol dehydration into alkenes would be essentially catalyzed by the support over pairs of acidic and basic sites. Several mechanisms were proposed involving alkoxide or carboxylate adsorbed species [10,65,73–75]. Ethylene formation from ethanol could occur via an E_{1cB} mechanism involving both a weak Lewis acid site and a strong Brønsted basic site [75–77]. However, such a mechanism may also lead to the dehydrogenation of ethanol into acetaldehyde and cannot explain the catalyst selectivity [75]. Most probably this mechanism would explain the preferential dehydration of 2-alkanols into 1-alkenes instead of 2-alkenes [77]. A second mechanism for the dehydration (E_2 mechanism) is often proposed to explain most of the results observed on oxides. It implies a pair of acidic and basic sites that would be more equilibrated in strength [75]. However, whatever the mechanism, it has been well known since the 1960s that alcohol dehydration is much faster over acidic oxides than over basic oxides [78]. It can be concluded that, although O^{2-} ions intervene in the alcohol adsorption, the strength of the acid sites is a determining factor in the reaction kinetics. Intermolecular dehydration may also lead to the formation of ethers. However, it seems that this reaction essentially occurs at low temperature [79] and not upon ethanol steam reforming at 700 °C.

The different mechanisms proposed for ethanol dehydrogenation proceed via H abstraction on the C atom bearing the OH group (Hα) [65,75]. The strength of the basic site is then an essential parameter for this determining step. There are many indications in the literature that the selectivity for aldehydes (or ketones) is closely linked with the basic site strength of the oxide, provided that the number of weak acidic sites at the surface is sufficient [65,75,80]. The presence of these weak acidic sites is a key point in ethanol dehydrogenation, much more than for the dehydrogenation of heavier alcohols. Pure MgO, for instance, is poorly active in acetaldehyde production from ethanol [75], whereas it is significantly active in acetone production from 2-propanol [76] and in cyclohexanone production from cyclohexanol [65]. However, a few Al ions added to MgO are sufficient to make the solid very active in ethanol dehydrogenation to acetaldehyde [75].

Alcohol dehydrogenation can also be catalyzed by metals, especially Rh, Pt, and Pd [81]. Fatsikostas and Verykios [50] showed that γ-Al_2O_3 was very selective for ethylene, whereas La_2O_3 was rather selective for acetaldehyde, in agreement with the stronger basicity of lanthana. Ni added to the supports shifted all of the reactions toward lower temperatures and promoted the oxidation to CO and CO_2 and the formation of hydrogen. The authors showed, however, that Ni/Al_2O_3 was able to produce acetaldehyde, although this aldehyde was never observed on the bare alumina. In conclusion, it was proved that the dehydrogenation reaction mainly occurred (if not totally) on the metal.

In summary, the acidic and basic properties of the supports are essential parameters directly affecting the primary selectivity for acetaldehyde or ethylene. Acetaldehyde would be produced on both the support and the metal. Basic sites are predominant in the ethanol dehydrogenation. Ethylene would be produced only on the support, with an essential role of the acidic sites in olefin formation.

4.3. Role of the metal in the ethanol steam reforming reaction

According to the mechanisms previously described for the hydrocarbons [43] or ethanol steam reforming [5], the metal would activate the organic molecule and promote the reaction between the adsorbed CH_xO_y fragments with the OH groups from the support. Undoubtedly, Rh is the best metal in this role. Furthermore, many indications in the literature tend to demonstrate that the hydrocarbon or ethanol activation occurs more readily on small particles than on big ones. As discussed in Section 4.2, the primary reactants in the ethanol steam reforming were acetaldehyde and/or ethylene rather than the ethanol itself. The reaction of these two molecules with OH groups primarily led to CO and methane (Fig. 3). A similar mechanism was reported by Polychronopoulou et al. for phenol steam reforming over MgO-based supported Rh catalysts [82]. The secondary production of CO_2 is a general feature in ethanol steam reforming. Although CO_2 and CH_4 are thermodynamically stable products at low temperature, ethanol decomposition into $CO + CH_4 + H_2$ (Eq. (7)) could be kinetically favored.

This possibility would explain the formation of methane in the very first seconds of the reaction, even at relatively low temperature. The results reported by Galvita et al. for Pd/C at 200–400 °C confirm this general trend in ethanol steam reforming [83]. Then it might be concluded that methane is essentially formed via the direct decomposition of ethanol and probably not from CO methanation. Furthermore, CO_2 would originate from CO via the water gas shift reaction (WGSR). In turn, Rh is a poor WGS catalyst [52,84]. Grenoble et al. [84] reported the following order for the activity of various alumina-supported metal catalysts in the WGSR (TOF in h^{-1} at 300 °C): Cu (43400) > Re (1380) > Co (890) > Ru (695) > Ni (370) > Pt, Os (225) > Au (130) > Fe, Pd (50) > Rh (31) > Ir (12). As a rule, noble metals are not very active in the WGSR. Except for Ru, Pt is the best noble metal for the WGSR. Grenoble also showed that the reaction was extremely support-sensitive. The proposed explanation was the occurrence of an associative mechanism via surface formate species. Even though the mechanism and the nature of the intermediate species involved in the reaction remain questionable, several studies confirmed the crucial role of the support in the reaction [52,85,86]. In spite of the high temperature, Fig. 3 clearly demonstrates that WGS is not a fast reaction under the selected ethanol steam reforming conditions. Furthermore, CO or CO_2 methanation does not seem to be the main reaction path to methane. In any event, the promotion of such a reaction is not recommended. In contrast, the WGS activity should be improved to increase the H_2 yield at high space velocity (short contact time).

5. Conclusions

Rh is the most active metal in the steam reforming reaction, especially in ethanol steam reforming (ESR). However, the support plays a significant role:

(i) it should favor a good Rh stability.
(ii) it should be hydrophilic to promote water activation and possess very mobile OH groups to favor the reaction with the CH_xO_y fragments adsorbed on the metal particles.
(iii) it should favor ethanol dehydrogenation to acetaldehyde instead of alcohol dehydration to ethylene, to prevent coke formation.

All of these conditions plead in favor of a support that is non-acidic and moderately basic. MgAl-based spinels deposited on alumina beads were shown to be adequate supports for Rh in the ethanol steam reforming (ESR) reaction at 700 °C. The spinel layer was introduced to control the acidic and basic properties of the support and to improve the stability of the rhodium particles upon reaction. Compared with the alumina-supported catalysts, spinel-supported catalysts exhibited a slightly higher basicity, whereas the surface acidity was strongly reduced. The catalysts derived from the spinel prepared by solid–solid reaction between MgO and the alumina bead at 1000 °C (second generation) exhibited optimal performances. Although the catalysts were calcined at 700 °C before reduction at 500 °C, the rhodium precursor salt still had a substantial impact on the acidic and basic properties of the final catalyst. Rh acetate appeared to induce the lowest acidity (lower than the starting spinel/alumina support), whereas nitrate dramatically increased the overall acidity of the catalyst. Impregnation with Rh chloride was a good compromise, since we could obtain a very good dispersion of the metal without a significant increase in the solid acidity.

XRD and electron microscopy led to a schematic picture of the support where the alumina grains (about 40 nm), which constitute the beads, were coated with a rather regular spinel layer of about 8–9 nm. The thickness of the spinel layer was larger on the alumina grains located at the bead periphery than in the core. As a direct result, Rh would be preferentially impregnated on the spinel and not on the alumina.

$Mg_xNi_{1-x}Al_2O_4/Al_2O_3$-supported rhodium catalysts, in which the magnesium was partly replaced by Ni ions, showed excellent performances in the ESR at atmospheric pressure, whereas the pure MgAl spinel should be preferred for the ESR at moderate pressure (11 bar). Such conditions are required for the operation of the membrane H_2 purifier. Hydrogen yields as high as 550 $g_{H_2}\ h^{-1}\ g_{Rh}^{-1}$ were obtained, and the catalyst appeared to be fairly stable. The catalyst activity in the WGSR could be a limiting factor in obtaining the maximum H_2 yield at the highest space velocity.

Acknowledgments

The authors thank the ADEME (French National Agency for Environment and Energy Management) for financial support (contract 00 01 076). Special thanks are due to Etienne Poitrat for his advice in the field of biofuels and his constant support for the present study.

Appendix A

Alumina beads are assimilated to spheres of radius $r = 2$ mm. Each bead might be formally divided into spheres or shells of radius $r/4$, $r/2$, $3r/4$, and r to define four elementary volumes, $V_1 = (\pi r^3)/48$ (inner sphere), $V_2 = (7\pi r^3)/48$, $V_3 = (19\pi r^3)/48$, and $V_4 = (37\pi r^3)/48$ (spherical shells). It is verified that $V = \sum_{i=1}^{4} V_i = (4/3)\pi r^3$.

Furthermore, if one assumes α is the average Mg content in V_1, one may extract from Fig. 6 that the average concentration in Mg is 1.14α in V_2, 1.64α in V_3, and 2.52α in V_4. Assuming the global Mg content is 4.60%, the mass balance in Mg in the whole bead gives (after simplification by $\pi r^3/48$)

$$2.53\alpha \times 37 + 1.64\alpha \times 19 + 1.14\alpha \times 7 + \alpha = 4.60 \times 64,$$

i.e.,

$$\alpha = 2.207.$$

Then, the Mg content in each of the four elementary volume is 2.21% in V_1, 2.51% in V_2, 3.62% in V_3, and 5.58% in V_4.

Finally, each bead consists of an agglomeration of alumina grains (radius r_g) coated with the Mg spinel. In fact, magnesia reacted with the alumina grains to form an outer shell made of the $MgAl_2O_4$ spinel with a thickness ε. If one assumes the coating of the alumina grains is homogeneous and the Mg content in V_i is the same in every bead, we obtain

$$\text{Mg (\%)} = 100 \times \frac{24.3[1-(1-\varepsilon/r_g)^3]}{102+40.3[1-(1-\varepsilon/r_g)^3]}.$$

The resolution of this equation leads to $\varepsilon/r_g = 0.0332$ in V_1 (core), 0.0381 in V_2, 0.0571 in V_3, and 0.0947 in V_4 (outer shell). These calculations are based on a stoichiometry ratio in the spinel $y = \text{Al}/2\text{Mg}$ of 1.

For $y \approx 3$ ($Mg_{0.388}Al_{2.408}O_4$), $\varepsilon/r_g = 0.107$ in V_1, 0.125 in V_2, 0.198 in V_3, and 0.391 in V_4.

References

[1] S. Freni, G. Maggio, S. Cavallaro, J. Power Sources 62 (1996) 67.
[2] A.N. Fatsikostas, D.I. Kondarides, X.E. Verykios, Chem. Commun. (2001) 851.
[3] A.N. Fatsikostas, D.I. Kondarides, X.E. Verykios, Catal. Today 75 (2002) 145.
[4] S. Freni, S. Cavallaro, N. Mondello, L. Spadaro, F. Frusteri, J. Power Sources 108 (2002) 53.
[5] F. Auprêtre, C. Descorme, D. Duprez, Catal. Commun. 3 (2002) 263.
[6] D. Srinivas, C.V.V. Satyanarayana, H.S. Potdar, P. Ratnasamy, Appl. Catal. A 246 (2003) 323.
[7] J. Comas, F. Marino, M. Laborde, N. Amadeo, Chem. Eng. J. 98 (2004) 61.
[8] J. Sun, X. Qiu, F. Wu, W. Zhu, W. Wang, S. Hao, Int. J. Hydrogen Energy 29 (2004) 1075.
[9] F. Frusteri, S. Freni, V. Chiodo, L. Spadaro, O. Di Blasi, G. Bonura, S. Cavallaro, Appl. Catal. 270 (2004) 1.
[10] A.N. Fatsikostas, X.E. Verykios, J. Catal. 225 (2004) 439.
[11] F.J. Marino, E.G. Cerrella, S. Duhalde, M. Jobbagy, M.A. Laborde, Int. J. Hydrogen Energy 23 (1998) 1095.
[12] F. Marino, M. Boveri, G. Baronetti, M. Laborde, Int. J. Hydrogen Energy 26 (2001) 665.
[13] V. Klouz, V. Fierro, P. Denton, H. Katz, J.P. Lisse, S. Bouvot-Mauduit, C. Mirodatos, J. Power Sources 105 (2002) 26.
[14] V. Fierro, V. Klouz, O. Akdim, C. Mirodatos, Catal. Today 75 (2002) 141.
[15] S. Velu, N. Satoh, C.S. Gopinath, K. Suzuki, Catal. Lett. 82 (2002) 145.
[16] F. Marino, G. Baronetti, M. Jobbagy, M. Laborde, Appl. Catal. A 238 (2003) 41.
[17] F. Haga, T. Nakajima, H. Miya, S. Mishima, Catal. Lett. 48 (1997) 223.
[18] J. Llorca, N. Homs, J. Sales, P. Ramirez de la Piscina, J. Catal. 209 (2002) 306.
[19] J. Llorca, J.-A. Dalmon, P. Ramirez de la Piscina, N. Homs, Appl. Catal. A 243 (2003) 261.
[20] M.S. Batista, R.K.S. Santos, E.M. Assaf, J.M. Assaf, E.A. Ticianelli, J. Power Sources 124 (2003) 99.
[21] M.S. Batista, R.K.S. Santos, E.M. Assaf, J.M. Assaf, E.A. Ticianelli, J. Power Sources 134 (2004) 27.
[22] F. Frusteri, S. Freni, L. Spadaro, V. Chiodo, G. Bonura, S. Donato, S. Cavallaro, Catal. Commun. 5 (2004) 611.
[23] J. Llorca, N. Homs, J. Sales, J.-L.G. Fierro, P. Ramirez de la Piscina, J. Catal. 222 (2004) 470.
[24] A. Kaddouri, C. Mazzocchia, Catal. Commun. 5 (2004) 339.
[25] S. Cavallaro, S. Freni, Int. J. Hydrogen Energy 21 (1996) 465.
[26] S. Cavallaro, Energy Fuels 14 (2000) 1195.
[27] T. Rampe, P. Hubner, B. Vogel, A. Heinzel, in: Proc. 1st World Conference on Biomass for Energy and Industry, Sevilla, Spain, 5–9 June 2000, Science Publishers Ltd., 2001, p. 1889.
[28] S. Freni, J. Power Sources 94 (2001) 14.
[29] J.P. Breen, R. Burch, H.M. Coleman, Appl. Catal. B 39 (2002) 65.
[30] C. Diagne, H. Idriss, A. Kiennemann, Catal. Commun. 3 (2002) 565.
[31] D.K. Liguras, D.I. Kondarides, X.E. Verykios, Appl. Catal. B 43 (2003) 345.
[32] S. Cavallaro, V. Chiodo, S. Freni, N. Mondello, F. Frusteri, Appl. Catal. A 249 (2003) 119.
[33] S. Cavallaro, V. Chiodo, A. Vita, S. Freni, J. Power Sources 123 (2003) 10.
[34] F. Auprêtre, C. Descorme, D. Duprez, Stud. Surf. Sci. Catal. 145 (2003) 303.
[35] J. Rasko, A. Hancz, A. Erdohelyi, Appl. Catal. A 269 (2004) 13.
[36] F. Frusteri, S. Freni, L. Spadaro, V. Chiodo, G. Bonura, S. Donato, S. Cavallaro, Catal. Commun. 5 (2004) 611.
[37] F. Auprêtre, C. Descorme, D. Duprez, Top. Catal. 30 (2004) 487.
[38] E.C. Wanat, K. Venkataraman, L.D. Schmidt, Appl. Catal. A 276 (2004) 155.
[39] C. Diagne, H. Idriss, K. Pearson, M.A. Gomez-Garcia, A. Kiennemann, C.R. Chimie 7 (2004) 617.
[40] E. Kikuchi, K. Ito, T. Ino, Y. Morita, J. Catal. 46 (1977) 382.
[41] D. Duprez, P. Pereira, A. Miloudi, R. Maurel, J. Catal. 75 (1982) 151.
[42] H. Muraki, Y. Fujitani, Appl. Catal. 47 (1989) 75.
[43] D. Duprez, Appl. Catal. 82 (1992) 111.
[44] K. Kusakabe, K.-I. Sotowa, T. Eda, Y. Iwamoto, Fuel Proc. Technol. 86 (2004) 319.
[45] G. Kolb, R. Zapf, V. Hessel, H. Löwe, Appl. Catal. A 277 (2004) 155.
[46] J.R. Rostrup-Nielsen, J. Catal. 31 (1973) 173.
[47] D.C. Grenoble, J. Catal. 51 (1978) 212.
[48] D. Duprez, A. Miloudi, J. Little, J. Bousquet, Appl. Catal. 5 (1983) 219.
[49] D. Duprez, A. Miloudi, L. Tournayan, Appl. Catal. 14 (1985) 333.
[50] A.N. Fatsikostas, X.E. Verykios, J. Catal. 225 (2004) 439.
[51] J. Llorca, N. Homs, P. Ramirez de la Piscina, J. Catal. 227 (2004) 256.
[52] J. Barbier Jr., D. Duprez, Appl. Catal. B 3 (1993) 61.
[53] J. Barbier Jr., D. Duprez, Appl. Catal. B 4 (1994) 105.
[54] A.C.S.C. Teixeira, R. Giudici, Chem. Eng. Sci. 54 (1999) 3609.
[55] C.L. Pieck, C.R. Vera, E.M. Peirotti, J.C. Yori, Appl. Catal. A 226 (2002) 281.
[56] J. Sehested, J. Catal. 217 (2003) 417.
[57] I. Aartun, T. Gjervan, H. Venvik, O. Görke, P. Pfeifer, M. Fathi, A. Holmen, K. Schubert, Chem. Eng. J. 101 (2004) 93.
[58] H.C. Yao, S. Japar, M. Shelef, J. Catal. 50 (1977) 407.
[59] D. Duprez, A. Miloudi, G. Delahay, J. Grimblot, J. Chim. Phys. 83 (1986) 465.
[60] R.W. McCabe, R.K. Usmen, K. Ober, H.S. Gandhi, J. Catal. 151 (1995) 385.
[61] R. Burch, P.K. Loader, N.A. Cruise, Appl. Catal. A 147 (1996) 375.
[62] C.-P. Hwang, C.-T. Yeh, Q. Zhu, Catal. Today 51 (1999) 93.
[63] R. Polvinen, M. Vippola, M. Valden, T. Lepistö, A. Suopanki, M. Härkönen, J. Catal. 226 (2004) 372.
[64] S. Karmal, D. Duprez, G. Perot, J. Catal. 130 (1991) 212.
[65] D. Martin, D. Duprez, J. Mol. Catal. 118 (1997) 113.
[66] A. Corma, C. Rodellas, V. Fornes, J. Catal. 88 (1984) 374.
[67] C. Lahousse, A. Aboulayt, F. Maugé, J. Bachelier, J.C. Lavalley, J. Mol. Catal. 84 (1993) 283.

[68] M. Ziolek, J. Kujawa, O. Saur, A. Aboulayt, J.C. Lavalley, J. Mol. Catal. 112 (1996) 125.
[69] T. Onfroy, G. Clet, M. Houalla, Chem. Commun. (2001) 1378.
[70] T. Armaroli, M. Bevilacqua, M. Trombetta, A. Gutièrrez Alejandre, J. Ramirez, G. Busca, Appl. Catal. A 220 (2001) 181.
[71] C. Morterra, C. Cerrato, G. Meligrana, Langmuir 17 (2001) 7053.
[72] H. Knözinger, P. Ratnasamy, Catal. Rev. Sci. Eng. 17 (1978) 31.
[73] E.C. DeCanio, V.P. Nero, J.W. Bruno, J. Catal. 135 (1992) 444.
[74] E.C. DeCanio, J.W. Bruno, V.P. Nero, J.C. Edwards, J. Catal. 140 (1993) 84.
[75] J.I. DiCosimo, V.K. Diez, M. Xu, E. Iglesia, C.R. Apesteguia, J. Catal. 178 (1998) 499.
[76] V.K. Diez, C.R. Apesteguia, J.I. DiCosimo, J. Catal. 215 (2003) 220.
[77] P. Canesson, M. Blanchard, J. Catal. 42 (1976) 205.
[78] L. De Mourgues, F. Peyron, Y. Trambouze, M. Prettre, J. Catal. 7 (1967) 117.
[79] B. Shi, B.H. Davis, J. Catal. 157 (1995) 359.
[80] A.L. McKenzie, C.T. Fishel, R.J. Davis, J. Catal. 138 (1992) 547.
[81] M. Dobrovolszky, P. Tétényi, Z. Paál, J. Catal. 74 (1982) 31.
[82] K. Polychronopoulou, J.L.G. Fierro, A.M. Efstathiou, J. Catal. 228 (2004) 417.
[83] V.V. Galvita, G.L. Semin, V.D. Belyaev, V.A. Semikolenov, P. Tsiakaras, V.A. Sobyanin, Appl. Catal. 220 (2001) 123.
[84] D.C. Grenoble, M.M. Estadt, D.F. Ollis, J. Catal. 67 (1981) 90.
[85] P. Panagiotopoulou, D.I. Kondarides, J. Catal. 225 (2004) 327.
[86] A. Goguet, F.C. Meunier, D. Tibiletti, J.P. Breen, R. Burch, J. Phys. Chem. B 108 (2004) 20240.